



HAL
open science

Distinguishing Engineered TiO₂ Nanomaterials from Natural Ti Nanomaterials in Soil Using spICP-TOFMS and Machine Learning

Garret Bland, Matthew Battifarano, Ana Elena Pradas del Real, Géraldine Sarret, Gregory Lowry

► **To cite this version:**

Garret Bland, Matthew Battifarano, Ana Elena Pradas del Real, Géraldine Sarret, Gregory Lowry. Distinguishing Engineered TiO₂ Nanomaterials from Natural Ti Nanomaterials in Soil Using spICP-TOFMS and Machine Learning. *Environmental Science and Technology*, 2022, 56 (5), pp.2990-3001. 10.1021/acs.est.1c02950 . hal-03859338

HAL Id: hal-03859338

<https://hal.science/hal-03859338>

Submitted on 18 Nov 2022

HAL is a multi-disciplinary open access archive for the deposit and dissemination of scientific research documents, whether they are published or not. The documents may come from teaching and research institutions in France or abroad, or from public or private research centers.

L'archive ouverte pluridisciplinaire **HAL**, est destinée au dépôt et à la diffusion de documents scientifiques de niveau recherche, publiés ou non, émanant des établissements d'enseignement et de recherche français ou étrangers, des laboratoires publics ou privés.

1 Distinguishing Engineered TiO₂ Nanomaterials from Natural Ti Nanomaterials in soil using
2 spICP-TOFMS and Machine Learning

3 Garret D. Bland^{†, §}, Matthew Battifarano[†], Ana Elena Pradas del Real^{‡, 1} Géraldine Sarret[‡], and
4 Gregory V. Lowry^{†, §, *}

5 [†]Department of Civil and Environmental Engineering, Carnegie Mellon University, Pittsburgh,
6 Pennsylvania 15213, United States

7 [‡]ISTerre (Institut des Sciences de la Terre), Univ. Grenoble Alpes, CNRS, 38000, Grenoble,
8 France

9 [§]Center for Environmental Implications of NanoTechnology (CEINT), Carnegie Mellon
10 University, Pittsburgh, Pennsylvania 15213, United States

11 ¹Present Address: Madrid Institute for Agricultural Research (IMIDRA), N-II km 38,200,
12 28800 Alcala de Henares

13 **ABSTRACT:**

14 Identifying engineered nanomaterials (ENMs) made from earth-abundant elements in soils
15 is difficult because soil also contains natural nanomaterials (NNMs) containing similar elements.
16 Here, machine learning models using elemental fingerprints and mass distributions of three TiO₂
17 ENMs and Ti-based NNMs recovered from three natural soils measured by single particle
18 Inductively Coupled Plasma Time-Of-Flight Mass Spectrometry (spICP-TOFMS) was used to
19 identify TiO₂ ENMs in soil. Synthesized TiO₂ ENMs were unassociated with other elements
20 (>98%), while 40% of Ti-based ENM particles recovered from wastewater sludge had
21 distinguishable elemental associations. All Ti-based NNMs extracted from soil had a similar
22 chemical fingerprint despite the soils being from different regions, and > 60% of Ti-containing
23 NNMs had no measurable associated elements. A machine learning model best distinguished

24 NNMs and ENMs when differences in Ti-mass distribution existed between them. A trained LR
25 model could classify 100nm TiO₂ ENMs at concentrations of 150 mg kg⁻¹ or greater. The presence
26 of TiO₂ ENMs in soil could be confirmed using this approach for most ENM-soil combinations,
27 but the absence of a unique chemical fingerprint in a large fraction of both TiO₂ ENMs and Ti-
28 NNMs increases model uncertainty and hinders accurate quantification.

29 **Synopsis:**

30 We used elemental fingerprints and mass distribution of engineered TiO₂ nanoparticles and
31 naturally occurring natural Ti-containing nanoparticles and machine learning models to effectively
32 track and quantify Ti-based engineered nanomaterials (ENMs) in three different representative
33 soils.

34 **KEYWORDS:**

35 spICP-TOFMS, engineered nanomaterials, soil, sewage sludge, machine learning, classification,
36 TiO₂

37 **INTRODUCTION:**

38 ENMs are widely used in commercial and military applications (e.g. obscurants, armoring,
39 and self-healing materials) due to their unique properties.¹ Once applied, ENMs are inevitably
40 released into the environment which will continue to increase in the future.² For example, TiO₂
41 ENMs are a widely used nanomaterial that typically accumulates in municipal waste and sewers.^{3,4}
42 The released ENMs can potentially negatively impact ecosystem services such as food production
43 and nutrient cycling⁵ so accurate ENM risk assessments are needed. However, it is still a
44 significant challenge to identify the source of ENMs or to quantify the amount of a selected ENM
45 when present at environmentally relevant concentrations. This is especially true for ENMs made

46 from earth abundant elements like aluminum, silicon, iron, and titanium that are present in
47 environmental media at >1 wt% .^{6,7}

48 Distinguishing between ENMs and NNMs in environmental matrices like soil is difficult
49 using conventional analytical instrumentation, especially for ENMs made from earth abundant
50 elements. Electron Microscopy (TEM and SEM) can determine the morphology, crystallinity,
51 elemental composition, and sizes of ENMs in soils. However, it takes considerable effort to detect
52 ENMs via imaging without automation⁸, and can be impossible if ENMs are present in low
53 numbers. Inductively Coupled Plasma Mass Spectrometry (ICP-MS) measures the total metal
54 concentrations in environmental or biological media after sample digestion. Many studies have
55 used ICP-MS to track the fate of ENMs in soils⁹⁻¹¹ and plants¹²⁻¹⁴. However, this approach cannot
56 distinguish between metals in ENMs and background concentrations of those metals (particulate
57 or dissolved), especially at low ENM concentrations.^{15,16} Filtration and centrifugation can be used
58 to separate particulate and dissolved fractions, but the size cutoff is operationally-defined, and it
59 cannot fully distinguish dissolved and particulate measurements.¹⁷ Changes in the ratios of the
60 element of interest versus common earth elements (e.g. Ti and Al) relative to background ratios
61 have been used to indicate the presence of ENMs, but this cannot determine the specific source of
62 ENMs.^{4,8,18} Size separation techniques, such as field-flow fractionation (FFF), asymmetric flow
63 field-flow fractionation (A4F),¹⁹⁻²¹ size exclusion chromatography (SEC),²² and hydrodynamic
64 chromatography (HDC)¹¹ have been used to determine bulk metal concentration as a function of
65 particle size, but this does not determine single particle compositions. Single-particle Inductively
66 Coupled Mass Spectrometry (spICP-MS) can measure the mass of metal-based single
67 nanoparticles one element at a time,^{23,24} but many ENMs are made from earth-abundant elements
68 (e.g. Si, Al, Ce, Cu, Ti, and Fe)²⁵ making it difficult to distinguish them from the natural

69 nanomaterials (NNMs) in the sample that contain similar elements. Determining Ti-based ENM
70 concentrations is especially challenging since natural Ti is abundant in soils ranging from 0.2 to
71 2.4% worldwide.²⁶ Measuring multiple elements in each particle simultaneously may identify
72 differences in the chemical fingerprints between ENMs and NNMs.

73 Single-particle ICP Time-of-Flight Mass Spectrometry (spICP-TOFMS) can measure most
74 elements in the periodic table simultaneously on a single particle. This provides a rich data set
75 consisting of multi-elemental composition of thousands to tens of thousands of individual
76 nanoparticles in a sample in just a few minutes,²⁷ and can provide a specific elemental fingerprint
77 and mass distribution for each particle. For example, Ce ENMs can be distinguished from Ce-
78 containing NNMs using a natural tracer (La) that is present in a fraction of Ce-containing NNMs
79 but not in Ce ENMs.²⁸ However, there are detection limits for each element measured by spICP-
80 TOFMS. This currently limits the lower bound of particle detection to 20 to 30 nm depending on
81 the element, and limits particle fingerprint information in both ENMs and NNMs. Many elements,
82 including Ta, Nb, Zr, and rare earth elements are often associated with natural sources of Ti and
83 may be a “fingerprint” for Ti-containing NNMs^{29,30} that is distinguishable from TiO₂ ENMs which
84 are relatively pure. Gondikas et al., specifically measured the fingerprint of Ti-containing NMs in
85 surface water with spICP-TOFMS found that Al, Fe, Mn, and Pb are present in Ti-containing
86 NMs.⁸ Baalousha et al., determined the elemental fingerprint of Ti-containing NNMs in three soils
87 using spICP-TOFMS.³¹ While these “fingerprints” could be used to differentiate between NNMs
88 and ENMs, analytical strategies are needed to statistically assess elemental fingerprint information
89 for thousands of nanoparticles in a sample and determine which, if any, can be used to classify
90 them as ENMs or NNMs.

91 Machine learning (ML) classification models learn from complex datasets to identify
92 important features and formulate classification criterion without domain knowledge. The most
93 critical aspect of ML models is the consideration of *all* information within the dataset with many
94 dimensions of the features that can capture important trends that may not be determined by simpler
95 regressions or associations. There are two major categories of ML algorithms: unsupervised and
96 supervised learning.³² Unsupervised learning discovers hidden patterns in unlabeled datasets that
97 forms correlations between features that considers all available information. Supervised learning
98 trains on labeled datasets and predicts labels on unseen data, e.g., classification. The performance
99 of a supervised learning model is measured by predicting on unseen labeled test datasets. ML is
100 increasingly being applied in environmental science with a few studies focusing on ENMs. One
101 study implemented a gradient decision tree with boosting classification (GBC) and recursive
102 feature elimination (RFECV) to distinguish natural and engineered Ce-containing nanoparticles.²⁸
103 Another study used linear discriminant analysis (LDA) to classify isotopic fingerprinting of SiO₂
104 NPs.³³ Both models handled only a limited number of features (i.e. elements or isotopes). For the
105 GBC model, they limited the model to 25 features (and reduced this to 17 with RFECV) and the
106 LDA model used two features at a time. While these models could classify ENMs and NNMs for
107 these particles, the ability to classify TiO₂ ENMs and other ENMs made from earth abundant
108 elements in soil may require different approaches. For example, features other than chemical
109 fingerprint such as mass distribution of particles may also be important for accurate classification.

110 The objective of this study is to determine the properties of Ti-based NNMs and ENMs that
111 can be used to identify a specific Ti-based ENM in soils with background Ti-based NNMs. We
112 first investigate how the mass (size) and elemental fingerprints measured by spICP-TOFMS of Ti-
113 based NNMs vary depending on soil type and how these potentially affect classification. Machine-

114 learning models are developed to distinguish two synthesized Ti ENMs (30 nm and 100nm) and
115 Ti-ENMs recovered from wastewater treatment plant sludge from background Ti-based NNMs
116 present in three types of soil. The model consists of a dimension reduction method (non-negative
117 matrix factorization, NMF) and a linear classification model (Logistic Regression, LR) with k-fold
118 validation. To determine the particle concentration detection limit of Ti-ENMs in soil, the trained
119 model is then applied to Ti-particles extracted from soils dosed with varying concentration of TiO₂
120 ENMs. The model uses both Ti mass distribution and elemental fingerprinting for classification
121 because a large portion of Ti-based NNMs do not have elemental associations. The model
122 performed the best with test cases that have significant Ti-mass difference between ENMs and
123 NNMs. While machine learning models are specific to the data they are trained on, our approach
124 can confirm the presence of a specific TiO₂ ENM in a soil with a measured fingerprint of Ti-
125 NNMs, but accurate quantification is not yet possible for TiO₂ ENMs with similar size
126 distributions as the Ti-based NNMs.

127 **METHODS**

128 **Experimental Design**

129 The elemental fingerprints and mass distributions of Ti-containing NNMs extracted from
130 three different soils and three Ti-based NMs from different sources (two commercially available
131 synthesized TiO₂ NPs and Ti-based NMs extracted from sewage sludge) were used to develop
132 machine learning models (3x3 matrix, Table S2) to classify between natural and engineered Ti-
133 based NMs in soil. While the two synthesized TiO₂ NPs are pristine “as manufactured” ENMs, the
134 Ti-based NMs extracted from wastewater sludge is more likely a unique mixture of ENMs and
135 NNMs. Therefore, we label the sludge as its own category, “Ti-sludge”. We refer to Ti-sludge as
136 an “ENM” to distinguish it from NNMs recovered from soils. The mass distributions and elemental

137 fingerprints were measured by spICP-TOFMS for each NM. To do this, the extracts from soil were
138 diluted with DI water, and ENMs were suspended and diluted in DI water. For the discussion of
139 this study, first the NNMs extracted from one soil is paired with the three different ENMs to
140 determine how ENM particle type affects the ability to classify them in a particular soil. Then, one
141 ENM type is paired with three different NNMs to understand if different natural backgrounds can
142 influence the classification of a particular ENM type. Therefore, five of the nine cases are
143 explained in detail in the results and discussion section while the remaining cases are explained in
144 SI (Figure S10). The limit of TiO₂ ENM detection was also approximated. This was done by adding
145 different known amounts of a TiO₂ ENM to a soil, extracting all NMs (<500 nm size fraction)
146 from soil using an established method, determining their mass distribution and elemental
147 fingerprints by spICP-TOFMS, and using the trained ML model to quantify the number of TiO₂
148 ENMs extracted from the soil.

149 **Materials and Samples**

150 Polyvinylpyrrolidone (PVP) 70 kg mol⁻¹, triethanolamine (TEA), diethylenetriamine
151 pentaacetate (DTPA), sodium chloride, and Triton X-114 were purchased from Sigma Adrich.
152 Carboxymethyl cellulose 700 kg mol⁻¹ was purchased from Acros Organics. All chemicals have a
153 purity of ≥ 99%.

154 Three types of Ti-based ENMs and three NNMs were used in this study. TiO₂ anatase
155 nanoparticles of a 30nm nominal size were purchased from US Research Nanomaterials (Ti30).
156 TiO₂ (rutile) nanoparticles with an average size of 100nm were provided by the US Army Research
157 Office (Ti100). Both ENMs were received as dry powders. The mineral phases for Ti100 were
158 confirmed by XRD (Figure S3). The mineral phase for Ti30 was determined from XRD and was
159 provided by the manufacturer. For the ENMs (Ti100 and Ti30), the particles were characterized

160 by TEM, DLS, and spICP-TOFMS (Table S1) in DI water. The suspensions were bath sonicated
161 for 30 minutes in an ice bath prior to characterization. The particle size and morphology were
162 determined by TEM using a JEOL JEM-2000EX and ImageJ software. The hydrodynamic
163 diameter of the ENMs was measured by a Malvern Zetasizer Nano ZS at 10 mg l^{-1} in 5 mM NaCl
164 with a pH of 5.6. The sewage sludge containing TiO_2 ENMs (Ti-sludge) was produced in a
165 wastewater treatment plant at Eawag (Zurich, Switzerland). Further details of the sludge are
166 provided in previous studies.^{34,35} ENMs could be introduced into terrestrial ecosystems through
167 the application of treated wastewater sludge so they represent an environmentally relevant input
168 of ENMs entering soils.³⁶ It is important to note that the Ti-based NMs in the sludge can be from
169 both natural and anthropogenic sources, but in TEM-EDX analysis, TiO_2 ENMs were identified.³⁵

170 NNMs were extracted from three types of soils: a loamy sandy soil (L22) (Lufa 2.2, Germany),
171 a loamy soil (LUV) (Luvisol, WRB, 2006) collected from La Côte Saint-André (Isère, France),
172 and a calcareous clayey loam soil (ARZ) collected from a plot at the Marcopa Agricultural Center
173 ($33^\circ 04' 22'' \text{ N}$, $111^\circ 58' 26.5'' \text{ W}$) in Arizona, USA.^{37,38} These soils were selected to provide a
174 range of geographical locations and soil properties (Table S2). LUV soil has the highest organic
175 carbon content (2.23%) followed by L22 and ARZ soil (1.71% and 0.54% respectively). L22 is
176 the most acidic soil (pH = 5.8) with LUV soil being circumneutral (pH = 6.4) and ARZ soil being
177 alkaline (pH = 7.6). Lastly, ARZ soil has the highest clay content compared to L22 and LUV soil.
178 We hypothesized that with different soil properties and source formations there would be distinct
179 Ti chemical fingerprint in each NNMs.

180 For spICP-TOFMS analysis, dissolved multi elemental standards (10 ppm) were purchased
181 from Inorganic Ventures. Tuning solution from Thermofisher containing 1 ppb of dissolved Co,
182 In, Ce, and U was used to calibrate the optics of the instrument and TOF detector. For the Au

183 nanoparticle standard, citrate capped Au nanoparticles (particle size = 50nm) were purchased from
184 Sigma Aldrich (particle size distribution by TEM = 49.1 ± 6.51 nm, number of particles = 193).

185 **ENM Dosing Procedure**

186 To approximate the detection limit of the method, Lufa 2.2 soil was dosed with Ti100
187 ENMs at nominal concentrations of 70, 150, 300, 700, and 7,000 mg-TiO₂ kg⁻¹ using previously
188 published methods to provide uniform mixing which is briefly described later.³⁹ The detection
189 limit in this instance is defined as the minimum ENM concentration in soil the model can
190 confidently predict and be statistically different from undosed soil. These dosed concentrations are
191 higher than what is predicted for soil with current material flow models, but the goal here is to
192 estimate the minimum ENM concentration needed for detection using our sample preparation and
193 ML model.⁴⁰ While the Ti100 ENM suspension was bath sonicated, an aliquot was pipetted and
194 evenly distributed in the soil to achieve field capacity moisture content (22%). The sample was
195 thoroughly mixed by wooden sticks for at least 15 minutes and transferred to a PTFE centrifuge
196 tube, loosely capped, and stored in dark for 24 hours to allow interaction with the matrix. The
197 samples were then subjected to the NM extraction procedure (details below). It is worth noting
198 that the 24-hour incubation time is relatively short and may not include long-term aging processes
199 that can affect extraction efficiency, e.g., heteroaggregation. However, the objective of this study
200 is to determine how well the ML model predicts ENM concentrations in impacted soils, and aging
201 effects were not considered in this study.

202 **Soil NM Extraction Procedure**

203 The <500 nm particles were extracted from soil and sludge using a previously described
204 method.³⁷ Briefly, the sediment was preconditioned with a NaCl solution at a 1:10 solid to liquid

205 ratio. The extraction solution is then added to the mixture containing carboxymethyl cellulose to
206 enhance the stabilization of nanoparticles against aggregation. This soil/solution mixture is
207 centrifuged at a particle size cut-off of 500 nm for soil assuming a bulk soil density of 2.65 g cm^{-3}
208 ³ (300 g for 5 mins using a JS 5.2 Swingbucket rotor). The supernatant containing the nanoparticles
209 goes through a cloud point extraction (CPE) enrichment step. A surfactant, Triton X-114, and NaCl
210 were added to the extract to achieve a final concentration of 0.2% and 10 mM, respectively. The
211 mixture was then heated at 40°C for 1 hour to form micelles. This was centrifuged to create a 2-
212 phase system: a surfactant-enriched phase containing the nanoparticles and water phase containing
213 the ions. The enriched surfactant phase containing nanoparticles was diluted and washed several
214 times by DI water and centrifugation. These samples were then stored in the dark at 4°C until
215 analysis.

216 **spICP-TOFMS**

217 The spICP-TOFMS 1R by TOFWERK (Zurich, Switzerland) is used for this study. For
218 ICP-TOFMS analysis, <500 nm extracted suspensions were diluted with DI water to 10^5 to 10^6
219 particles mL^{-1} for analysis. The samples were then bath sonicated for 8 minutes prior to
220 measurement. The instrument was calibrated from dissolved metal standards (Inorganic Ventures)
221 with a range from 10 ppt to 5 ppb in 1% trace-metal grade HNO_3 . The spICP-TOFMS tracks
222 multiple elements simultaneously during acquisition. Table S4 provides a list of optic and TOF
223 detector parameters. The spICP-TOFMS detector system is a microchannel plate detector (MCP)
224 converts the ion momentum into measurable signal. The TOF extraction frequency (extractions
225 per s) for all isotopes is 33 kHz. Then these extractions were averaged over an integration time of
226 2 ms to provide each data point. Shorter dwell times were tested but we did not observe any
227 significant difference in the single particle dataset. We also did not observe split-peak particles

228 after the correction (explained later). Particle coincidence could occur resulting in false positives
229 of multi-elemental particles. We predicted that a small fraction (less than 10%) of the multielement
230 particles could be false positive. Further discussion is provided in SI. The transport efficiency was
231 calculated using the size based method with a 50 nm Au nanoparticle suspension (Sigma Aldrich)
232 as previously described.⁴¹ Instead of the peak height, the peak area was used to measure Au-based
233 signal of the individual particle events.

234 Single particle processing was achieved using Python script provided by TOFWERK. This
235 process allowed for the detection of single particles from baseline signal. For each sample
236 acquisition, the mean and standard deviation signal of the sample was calculated for every isotope
237 in 100 integration time point intervals. Since each sample acquisition is made up of 60,020 data
238 points, the identification of single particle events is compartmentalized in discrete 100-time
239 intervals where the particle events are compared to localized background signal in the same
240 interval. The threshold for single particle detection follows the International Union of Pure and
241 Applied Chemistry (IUPAC) guideline to describe low intensity noise (threshold = $\mu + 3.29\sigma +$
242 2.72 , μ and σ is the average and standard deviation of signal intensity, respectively).⁴² Any
243 integration time point above this threshold is considered a single particle event. The detection limit
244 varies because the calculated threshold compared to background signal is different for each 100-
245 integration time point interval. Detection limits of single particles for every isotope can be
246 estimated by calculating the average threshold from background signal in each sample. For ⁴⁸Ti,
247 the average detection limit size of a TiO₂ particle (assuming a spherical shape and rutile density of
248 4.23 g cm⁻³) for all samples measure is approximately 36 nm which is on par or better than previous
249 spICP-MS studies.^{4,8,43,44} This is mainly due to the high dilution factor in DI water and low
250 background signal (0.01 to 0.02 $\mu\text{g L}^{-1}$). Once the single particles are identified, the baseline signal

251 average and standard deviation are recalculated. If more single particles are detected, then this
252 process is iterated up to 10 times before proceeding to the next window of 100 integration time
253 points. This is an iterative approach to ensure no outliers are found in background signal. Split-
254 peak particle events occur when a single particle event corresponds to multiple integration time
255 points. These signals are added together and are reported as a single particle event (maximum of
256 3 consecutive particle signals). Signal loss does not occur during split-peak particle events.

257 **Machine Learning Model**

258 Binomial Logistic Regression (LR) was used to classify ENMs and NNMs. The pipeline
259 of this model was written in Python Sci-Kit Learn Module. Other classification models were also
260 evaluated and compared to the LR results. This pipeline consists of three components: pretreatment
261 of the data set, training the classification model, and testing (Figure S1). The data set is comprised
262 of masses and elemental fingerprints from ENM and NNM samples measured by spICP-TOFMS
263 separately. Data from each of the six NMs analyzed are then parsed in Python to only include Ti-
264 particle events. For each ENM-NNM test case that is discussed in the “Experimental Design”
265 section and in Table S2, the single particle data from an ENM is randomly mixed with equal
266 portions of single particle data from an NNM (50% ENM and 50% NNM) to provide a balanced
267 dataset. Twenty percent of the mixed data is withheld as a test data set and remaining 80% is used
268 for training. Training datasets undergo a data transformation method called non-negative matrix
269 factorization (NMF). Similar to principal component analysis, the purpose of NMF is to reduce
270 the dimensionality of the given features (i.e., analytes) to 10 components while preserving all
271 elemental information. This dimensionality reduction technique is well-suited for single-particle
272 mass data because it requires all values to be non-negative. We also have varied the number of
273 components between 5, 10, 15, and 20 and found that 10 or higher provided the best performance

274 (Details in SI). In addition to the NMF components, a ^{48}Ti component was implemented, so the
275 model can consider Ti mass separately from other elements during classification. This enables the
276 model to use mass distribution and elemental fingerprint differences simultaneously. The LR
277 model is then trained on the dataset using five-fold cross validation and the limited-memory
278 Broyden-Fletcher-Goldfarb-Shanno (BFGS) algorithm as the solver.⁴⁵ To train, the LR model
279 optimizes the weight to each of the eleven components for the best classification performance. The
280 weights of the model components are then updated, and it reiterates this process until the algorithm
281 converges with a 0.001 tolerance stopping criteria. The trained model is then evaluated with the
282 test data set. Each test data point is given a probability of being ENM or NNM. This process is
283 done for every scenario between the three NNMs (Lufa 2.2, Luvisol, and Arizona) and the three
284 ENMs (Ti-sludge, Ti100, and Ti30), in total producing nine different trained models and predicted
285 scores. The particles are then assigned to three categories: classified ($\geq 85\%$ predicted probability
286 in the correct category), uncertain (between 15% and 85%), and incorrectly classified ($< 15\%$).
287 Table S2 displays which figure each test case results are in (Figure 3, 5, and S10). The 85% and
288 15% confidence level are *operationally defined* to categorize the test dataset and to compare all
289 cases. The importance of each element was calculated for each case and the top isotopes are listed
290 in SI (Figure S14, S15, and S16). The trained L22 + Ti100 model was then used to predict the
291 classification of extracted Ti-containing NMs from L22 soil dosed with 70, 150, 300, 700, and
292 7,000 mg kg⁻¹ of Ti100 ENMs. The model predicts the percentage of ENM particles in the dosed
293 soil. Python script for the spICP-TOFMS ML model, fingerprinting analysis, detection limits,
294 including figures are available in Github (github.com/gbland0725/sphandles/) and functionality
295 can be imported as a package via TestPypi (test.pypi.org/project/sphandles/).

296 **Total Ti concentration**

297 We determined the Ti concentration (mg kg^{-1} soil) in L22 soil without ENM addition and
298 after being dosed at 70, 700, and 7,000 mg kg^{-1} of Ti100 ENMs. We also measure the mass of
299 extracted Ti to calculate the extraction efficiency. The soil or the extracted NMs were oven dried
300 (60°C) for 48 hours and ground by mortar and pestle before analysis. Total Ti concentration was
301 determined by digestion followed by ICP-OES measurement as previously described.⁴⁶ Briefly,
302 20 to 30 mg of ground material is transferred to a 20 mL Teflon tube for chemical digestion. The
303 following mixture is added for digestion: 5 ml 70% HNO_3 , 0.2 ml HF (48%) and 0.5 mL H_2O_2
304 (30%). The sample is then microwaved in an MLS ultraclave. A reference soil (Canadian
305 Reference Soil SO-1) with a Ti content of 0.53% is also used to validate Ti concentrations which
306 are in a similar range to the other soils (0.32%, 0.27%, and 0.17% for ARZ, LUV, and L22 soil,
307 respectively). Ti recoveries of the reference soil was $89.9\% \pm 2.3\%$ ($n = 2$).

308 **Results and Discussion**

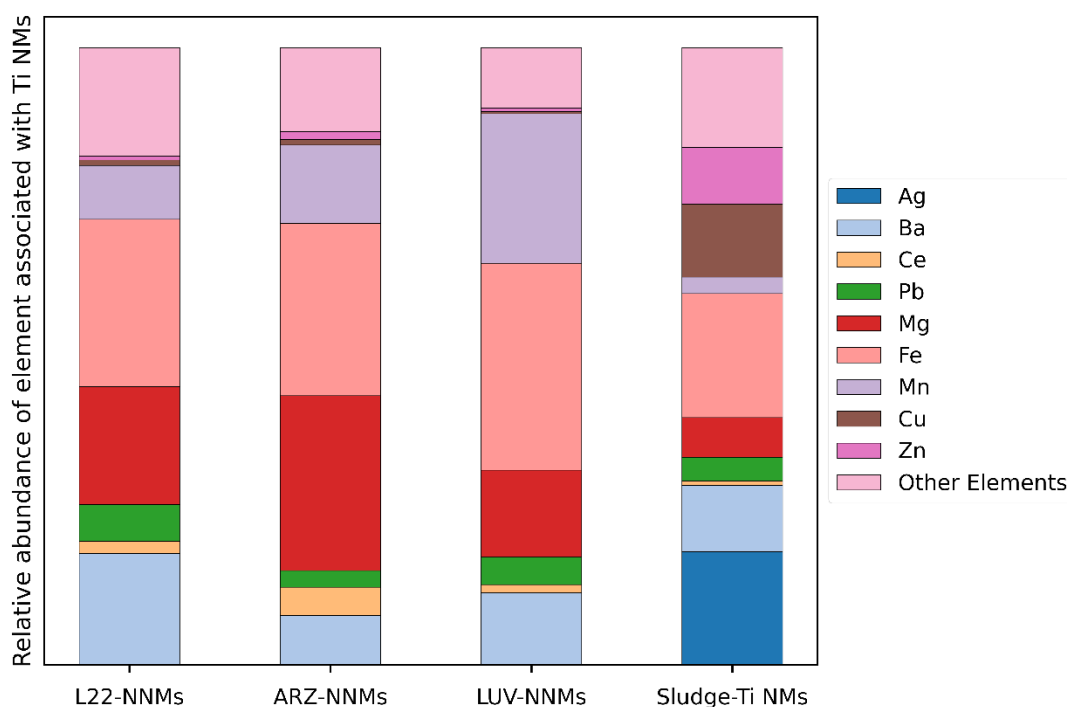
309 **Characterization: Elemental Fingerprints and mass distributions of the Ti-particles**

310 We determined the fraction of Ti particles in each sample with elemental associations and
311 the most common elements associated with Ti-containing particles for each NNM and ENM
312 (Figure 1). Elemental associations are defined as single element particle events identified within a
313 single dwell time point after split peak correction. For the NNMs in soil (LUV, L22, and ARZ),
314 between 20% to 35% of the Ti-particles were associated with other earth-abundant elements (e.g.,
315 Ce, Ba, Rb, Fe, Mg, Mn, Nb, and Pb). Often the Ti particles were associated with several different
316 elements. Interestingly, there were only minor differences between particles recovered from each
317 soil, despite that the soils were sourced from different regions and have different properties (Table
318 S2). We hypothesized that NNM in the L22 soil would have more differences because the acidic
319 pH and higher organic matter content could mobilize Ti into other soil particles. However, the

320 three soils used here do not likely represent all soil types. Importantly, there was a significant
321 fraction of Ti particles that were not associated with any other elements (80, 81, and 65% for ARZ,
322 L22, and LUV respectively). This is likely because the most common forms of titanium minerals
323 (TiO_2 , rutile and anatase) are resistant to weathering and have low solubilities.⁴⁷⁻⁴⁹ Isomorphic
324 substitution and incorporation of other elements into Ti-NMs are minimal and the morphology is
325 well preserved. Adsorption of another element (e.g., Fe) on the surface of the Ti-NMs is possible.
326 However, even if all the adsorption sites were saturated (one atom thick layer around a 100nm
327 TiO_2 sphere), the mass of the adsorbed element is not sufficient to be measured as a particle event
328 by the spICP-TOFMS because it would be below the detection limits (10^{-16} to 10^{-17} grams for most
329 elements). Previous studies have also reported the presence of <100 nm TiO_2 NNMs in soils and
330 sludge.^{35,50} Ti particles may have trace elements associated but given the detection limits of the
331 spICP-TOFMS, there may not be enough mass of the trace element to be recognized as a single
332 particle event.

333 For both pure synthesized ENMs (Ti100 and Ti30), there are negligible amounts of other
334 elements in the particles, as expected for an engineered material (> 98% of the particles were only
335 Ti). For the Ti-sludge (presumed to be primarily ENMs entering the treatment plant)³⁵, a large
336 fraction (65%) of Ti-particles are associated with other elements like Ag, Fe, and Pb. This is likely
337 because the Ti-containing particles are heteroaggregated with organic particles containing other
338 metals. The organic carbon content of the colloids from the sludge is $36.9 \pm 0.6\%$, and SEM images
339 from a previous study showed the TiO_2 particles embedded into organo-mineral
340 heteroaggregates.³⁵ A few elements were found in both NNMs and Ti-sludge particles, including
341 Fe, Mg, and Ba. However, there were also unique elements associated only with Ti-sludge
342 particles, including Cu, Ag, and Pb. The Ag attachment is high because this sludge was also

343 deliberately dosed with AgNPs.³⁴ Similar to the soils, there are also a substantial fraction of Ti
 344 particles (43% of the particles) that are not associated with other elements. Therefore, formulating
 345 a classification criterion based strictly on elemental fingerprint of Ti-containing particles will not
 346 be robust because of the significant number of Ti-particles without associated metals, and in the
 347 case of the Ti-sludge, because they have similar elemental associations as the soils.



348
 349 Figure 1: The fingerprints of multi-element Ti NNMs in L22, ARZ, LUV, and recovered Ti-NMs
 350 from Sludge. The major isotope except for Fe (⁵⁴Fe) is used to represent each element. Note that
 351 Ti30 and Ti100 are not shown because they had no element associations (pure Ti). Total values
 352 were calculated by the percentage of total Ti particles associated with each element. The values
 353 were then normalized to one to compare between samples. $\left(\frac{\% \text{ of element associated with Ti-NMs}}{\sum_{k=1}^{10} \% \text{ of element associated with Ti-NMs}} \right)$

354 The Ti particle mass distribution differences was also used for classification. The mass
 355 distribution of Ti-particle events was determined by spICP-TOFMS for each of the samples

356 (Figure S9). All Ti-based NNMs have a similar mass distribution, with medians of 1.78, 1.37, and
357 1.40×10^{-16} grams for ARZ, L22, and LUV, respectively. This correlated to sizes with mean and
358 standard deviation of 49.9 ± 22.5 nm, 49.3 ± 30.6 nm, and 48.8 ± 26.2 nm, respectively, assuming
359 spherical rutile particles. The similar median particle masses are possibly because most of the
360 identified Ti-particles are near the average IUPAC threshold, so smaller particles in the distribution
361 are not detected. The range of masses for the sludge Ti-particles is larger, from 10^{-16} to 10^{-13} grams.
362 For all samples, the range of mass distribution for Ti-particles without other associated metals is
363 similar to the overall Ti-mass distribution, indicating that the types of impurities associated with
364 the Ti particles is not dependent on Ti mass. The ENMs, Ti100 and Ti30, had narrow mass
365 distributions, and were slightly higher than the size range determined by TEM (Table S1).

366 **ML Model Selection and Comparison**

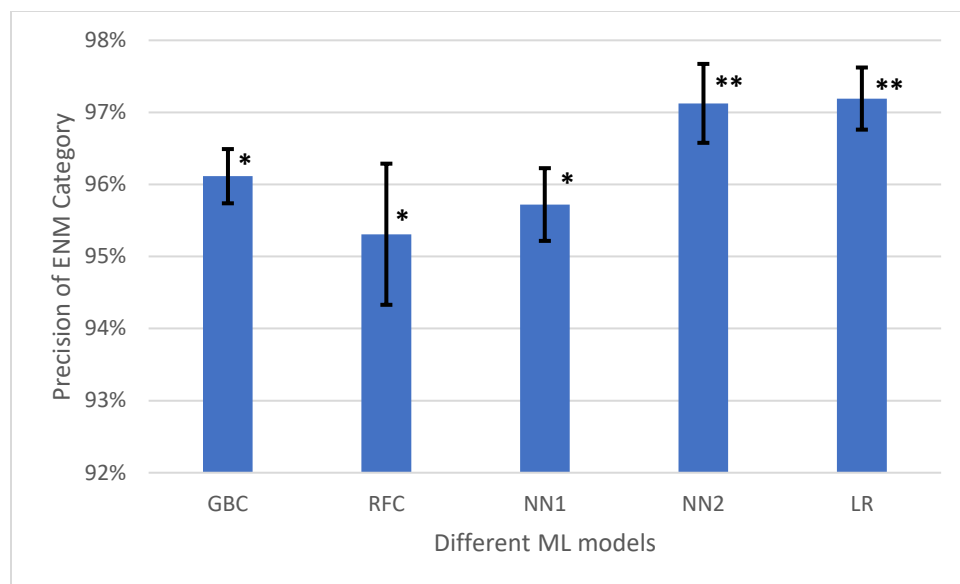
367 Different types of machine learning models were investigated to determine the most
368 appropriate for classification, including Gradient Boosting Classification (GBC), Random Forest
369 Classifier (RFC), and Neural Networks with either a 'relu' or 'logistic' activation layer (NN1 and
370 NN2, respectively). Performance is based upon training data from Ti100 and L22 case. The
371 average five-fold cross validation accuracy was used to compare each model and classification
372 was operationally assigned as $>85\%$ = correct, 15% to 85% = uncertain, and $<15\%$ = incorrect.
373 One major criterion for model selection is high precision of the ENM category: i.e., maximizing
374 the amount of ENMs predicted correctly while minimizing the amount of NNMs predicted
375 incorrectly as ENMs (false positive). All models exhibited similar trends as the LR model. The
376 major difference is the sensitivity of the mass discrimination difference between ENMs and
377 NNMs. GBC and RFC models had similar performance putting 80.6% of particles in the correct
378 category (i.e., above 85% confidence), about 2 times greater than the LR model (40%). However,

379 the percentage of incorrectly classified particles (4.6%) is also about 5 times higher than for the
380 LR model that has only 0.9% incorrect. NN1 also had a similar performance with 79.6% correct
381 and 4.2% incorrect. NN2 was similar to the LR performance at 39.1% correct and 0.9% incorrect
382 which is not surprising given the activation layer is the same mechanism (logistic function). The
383 greater number of false positives (i.e., NNM predicted as ENM) for the GBC and RFC models was
384 because they classified pure Ti particle events stochastically. This is evident from larger Ti100
385 ENMs classified below the 85% confidence level. Note, if the operationally defined classification
386 boundary was shifted to a 75% confidence level, the difference in performance between the models
387 was considerably smaller (Table S3). The NN models are similar to LR but can describe
388 nonlinearities within components which may produce overfitting and lose generalization of the
389 data. The highest precision of the ENM category was NN2 and LR. We conclude that the
390 performance of the models is primarily based on how the model weighted the Ti mass-
391 discrimination for the pure Ti-NNMs and decided to choose LR to minimize the number of
392 incorrect particle events and to determine the important features for each ENM + NNM case. All
393 models performed worse without including the mass distribution.

394 Table 1: The classification performance results of each ML model for the Ti100 + L22 Case.
395 (>85% = correct, 15% to 85% = uncertain, <15% = incorrect). Number of simulations = 9. Average
396 percentage values are reported with standard deviation in parentheses.

<i>Model Type</i>	<i>Certain (> 85%)</i>	<i>Uncertain (15% to 85%)</i>	<i>Incorrect (< 15%)</i>
<i>RFC</i>	80.7 (1.3)	14.9 (1.6)	4.5 (0.5)
<i>GBC</i>	81.5 (1.2)	14.5 (1.5)	4.1 (0.5)
<i>NN1</i>	82.3 (0.6)	13.3 (0.7)	4.4 (0.3)
<i>NN2</i>	38.3 (1.6)	60.7 (1.6)	0.9 (0.1)
<i>LR</i>	41.3 (1.8)	57.7 (1.9)	1.0 (0.2)

397



398

399 Figure 2: The precision of the ENM category for each ML model (number of simulations = 10)
 400 with a confidence interval of 95%. Symbols represent statistical similarity (One-way ANOVA,
 401 similarities contain a p-value $>10^{-2}$).

402 ML Models for distinguishing between Ti-based NNMs and ENMs

403 *Influence of ENM type on model performance*

404 The ML model was trained to distinguish between ENMs and NNMs. For this discussion,
 405 we first focus on the ability to distinguish each ENM (Ti30, Ti100, and Ti-sludge) from the Ti-
 406 based particles recovered from the L22 soil. Figure 3 displays the probability of correctly
 407 predicting the category of each Ti particle. Figure 3A displays specifically for the Ti100 + L22
 408 case, 3B shows the Ti30 + L22 case, and 3C shows the Ti-sludge + L22. For each test case, the
 409 left scatter plot depicts *only the Ti-NNMs* and their probability of being predicted as ‘Natural’ by
 410 the model as a function of Ti-mass. The right scatter plot displays *only Ti-ENMs* and their
 411 probability of being predicted as ‘Engineered’. The filled circle markers are Ti-NMs that are
 412 associated with at least one other element, while the open circle markers are Ti-NMs that are

413 unassociated with other elements (only ^{48}Ti or ^{48}Ti and ^{46}Ti). The pie chart on the right shows the
414 percentage of the total particles having a probability $> 85\%$ in the correct category as green,
415 uncertain ($< 85\%$ and $>15\%$) as orange, or incorrectly classified ($<15\%$) as red. The elemental
416 fingerprint for each test case was evaluated for comparison between correctly classified ($> 85\%$)
417 and the uncertain/incorrectly classified particles (Figure S11). We use both ^{46}Ti and ^{48}Ti for this
418 analysis. Because ^{48}Ti is the main isotope, we refer this as the total Ti and report ^{46}Ti separately.

419 The model performed best for the Ti100 + L22 (40.3% correctly classified). To better
420 understand the reasons for the correctly classified particle population, we separated the L22 NNMs
421 and Ti100 ENMs and plotted each as a function of Ti-mass (Figure 3a). For the L22 Ti-NNMs
422 (left scatter plot), two trends are prominent (a and b). One is a population of particles that creates
423 a sigmoidal curve below the 85% confidence level. The sigmoidal curve of Ti-NNMs below the
424 85% confidence level (orange markers) does not contain any elemental fingerprint information and
425 the model exclusively compares the Ti-mass to distinguish the NNMs from ENMs. Therefore, the
426 certainty of assignment as a Ti-NNM decreases as the Ti-mass increases (b). The second is the
427 population of particles that lie above the 85% confidence level, many at the 100% level, that are
428 independent of particle mass (a). These particles all have elemental fingerprints (e.g., Ba, Mg, V,
429 Nb) that are not found in the ENMs, and therefore are correctly assigned as an NNM. The
430 elemental fingerprint of the L22 Ti-NNMs are plotted in Figure S11A.

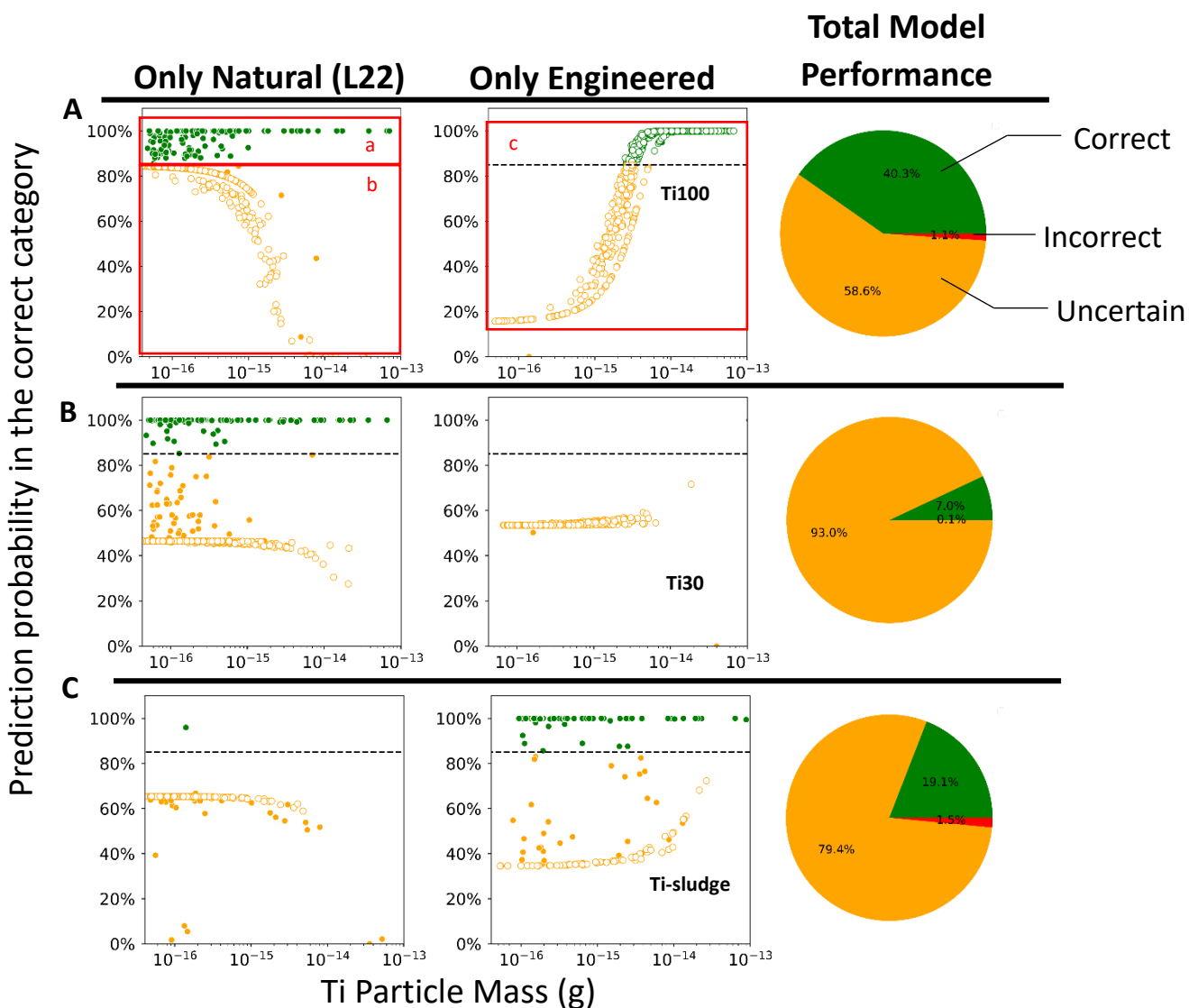
431 The right scatterplot contains only the Ti100 ENMs. The ENMs have no chemical
432 fingerprint so they lie on the sigmoidal curve. As the mass increased, so does the confidence that
433 they are correctly assigned as an ENM(c). Because of the mass difference between L22 and Ti100
434 (Figure 4), the model can correctly predict 68% of the Ti100 ENMs $>85\%$ confidence, making
435 Ti100 detectable in soil.

436 For the Ti30 + L22, the model does a poor job in its assignments (6.2% correctly classified
437 with a probability >85%). This is because the Ti-mass distribution for the ENMs and the NNMs
438 are overlapping (Figure 4). Therefore, the model uses only the L22 NNMs particles' elemental
439 fingerprint for classification. Figure 3b indicates that only Ti-containing NNMs that associate with
440 other elements are being correctly classified as such with confidence >85%, while the Ti30 ENMs
441 are indistinguishable. With the majority (80%) of L22 Ti-NNMs not having element associations,
442 and having a similar size to Ti30 ENMs, predicting any Ti30 ENM contribution in this soil is not
443 feasible.

444 For the Ti-sludge + L22 case (Figure 3c), the model performed adequately with 35% of the
445 Ti-sludge NMs being correctly classified with >85% confidence. Unlike the cases with “as
446 manufactured” ENMs, the NNMs in L22 soil were mostly classified as uncertain or incorrect with
447 a few outliers in the correct category when trying to distinguish them from the Ti-sludge NMs.
448 This is because the L22 Ti-NNMs that have elemental associations are also found in Ti-sludge
449 containing Mg, Mn, Pb, and Ba, so the model was not able to confidently distinguish them either
450 as ENMs or NNMs. The unique elemental associations in the Ti-sludge such as Sn, Ag, and Cu
451 (Figure S11D) led to a fraction of recovered Ti-NNMs having a high confidence regardless of Ti-
452 mass, but the model did allocate a small fraction of multi-element recovered Ti-NNMs that have Ag
453 between 50 and 85% confidence (Figure S13). Ti-sludge particles without elemental associations
454 follow a sigmoidal curve similar to the L22 + Ti100 case as a function of Ti-mass.

455 Nearly half of the Ti-sludge NMs had an elemental fingerprint. So, even though they have
456 an overlapping mass distribution with the Ti-based NNMs in L22, 35% of them were
457 distinguishable from the NNMs recovered from L22 soil. The lower amount of distinguishable
458 ENM particles (35%) than the amount with an elemental fingerprint (54%) indicates that the

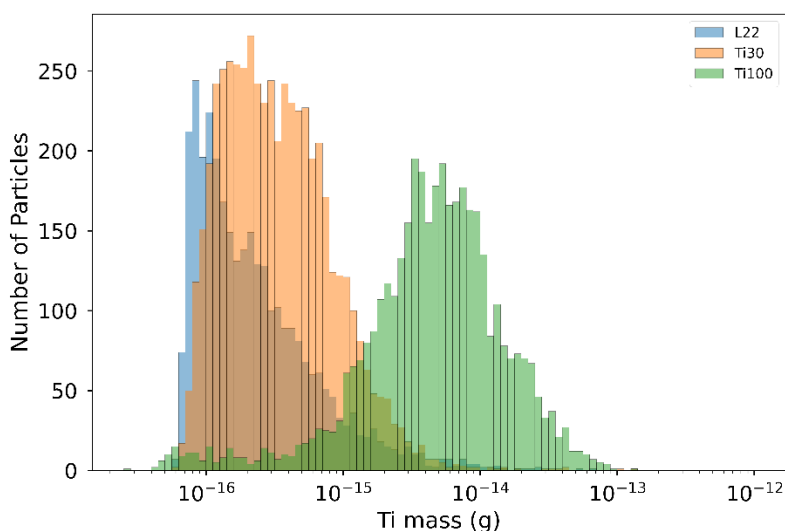
459 fingerprint was not unique enough to distinguish them from NNMs of soil. This may be because
460 the Ti-sludge particles are associating with organic sludge particles, giving them a similar
461 fingerprint. Previous studies have hypothesized that TiO₂ ENMs could attach to aluminosilicates
462 via heteroaggregation and would lead to detection of multiple elements in a single particle by
463 spICP-TOFMS but this warrants further investigation.^{51,52} In the testing set, there is also a
464 significant portion of Ti NNMs in the sludge (46%) and in L22 (81%) soil that do not have elemental
465 associations, but do have the same size distribution. This prevents higher model performance. Even
466 though the Ti-sludge particles cannot be fully classified in L22 soil, the model recognizes a specific
467 fingerprint and can distinguish a portion of Ti-sludge ENMs with high confidence.



469

470 Figure 3: Effect of engineered particle type on the ability to classify ENMs and NNMs. ML results
 471 are trained on training datasets and predicts on a held-out test dataset for the following test cases
 472 (A) Ti100 + L22, B) Ti30 + L22, and C) Ti-sludge + L22. For each test case, the left scatter plot
 473 shows *only Ti-NNMs* (L22) displayed as the probability of the ML model predicting the correct
 474 category (NNM) as a function of Ti mass. The right scatter plot displays *only the Ti-ENMs* as the
 475 probability of the ML model predicting the correct category (ENM) as a function of Ti mass. Green

476 represent Ti-NMs correctly classified (> 85%) and orange is uncertain or misclassified (<85%).
477 Filled circle markers are Ti-NMs with elemental associations and open circle markers are without
478 elemental association. These colors correspond to the elemental fingerprint information in SI
479 (Figure S11). The pie charts display the percentage of total Ti-NMs categorized as correct (green;
480 >85%), uncertain (orange; <85% and >15%), and incorrectly classified (red; <15%).



481
482 Figure 4: Comparing Ti-mass distribution between L22, Ti30, and Ti100. L22 and Ti30
483 significantly overlap while a clear separation exists between L22 and Ti100.

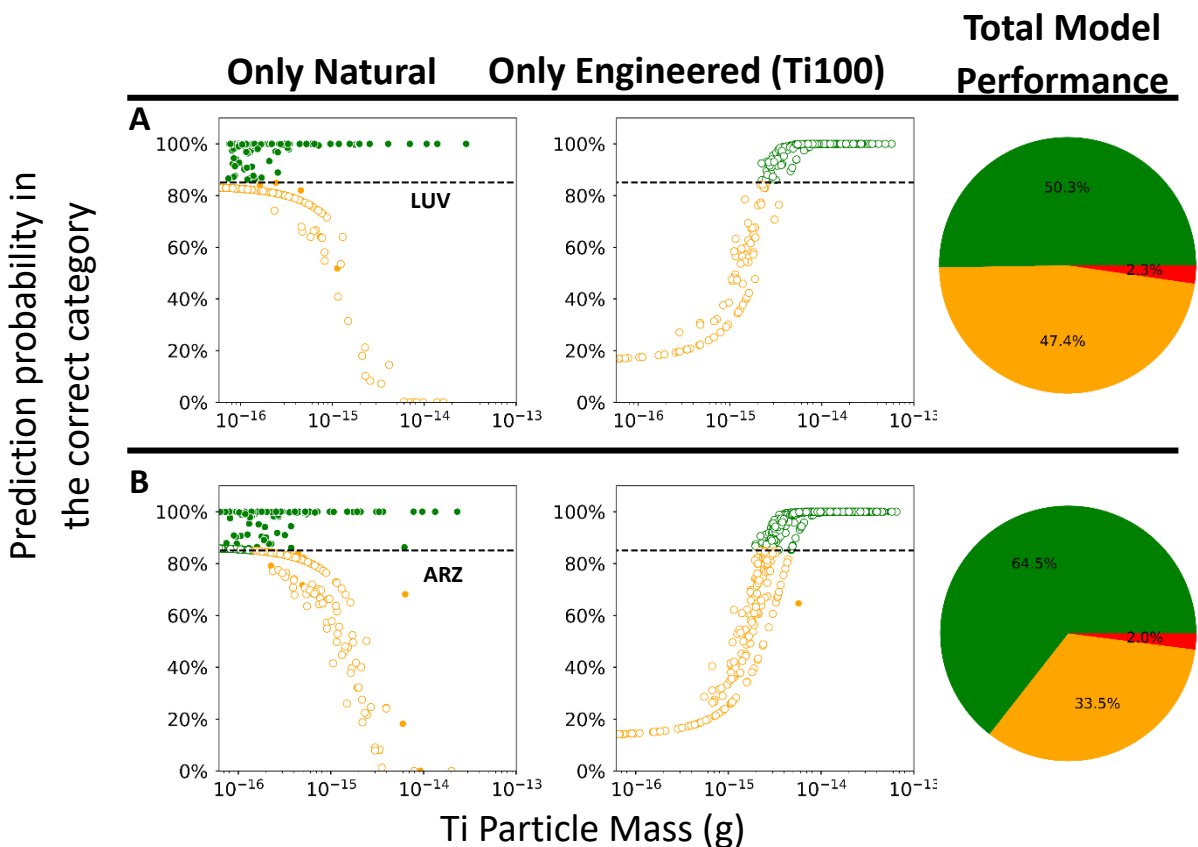
484 *Influence of Ti-NNM properties on ability to classify Ti-based ENMs*

485 The ability to classify Ti100 ENMs in each soil type was assessed to determine if
486 differences in elemental fingerprint and size distribution of the NNMs affected the ability to detect
487 the Ti100 ENMs. The model was able to classify the Ti100 ENMs in all three soils. The model
488 performed best for the Ti100 + ARZ (64.5%), followed by Ti100 + LUV (50.3%) and Ti100 +
489 L22 (40.3%) (Figure 4). Note that the Ti100 + L22 case is shown in Figure 3. For the ARZ case,
490 a portion of Ti-NNMs without elemental associations were classified correctly (> 85%) because

491 of their narrow mass distribution compared to LUV and L22. For the LUV case, there are more
492 Ti-NNMs that associate with other elements compared to L22, and therefore more particles were
493 correctly classified in the LUV soil compared to the L22 soil.

494 For all cases, the classification of the ENMs followed a sigmoidal curve which is expected
495 since Ti100 did not have any elemental associations and the model used Ti-mass only for
496 classification. The similar model results from the three cases reflects the similar elemental
497 fingerprint amount and mass distribution between the three NNMs, even though the soils are from
498 different locations and have different soil properties (Table S2). This is also reflected in the results
499 of the remaining four cases in SI (Figure S10)

500 The model also determines what elements are important and used to measure how size and
501 elemental fingerprint are weighted for each test case. The element importance is determined by a
502 LR model (Figure S14, calculations described in SI). For this calculation, the frequency of the
503 element within the sample is considered. For the L22 and ARZ soil cases, ^{46}Ti and ^{48}Ti are the
504 most important analytes for the prediction of a Ti-particle. This is expected because the model
505 identifies the significant Ti-mass differences to classify the two categories. The remaining analytes
506 are only identified in NNMs, such as ^{93}Nb , ^{25}Mg , ^{208}Pb , ^{57}Fe , ^{55}Mn , ^{90}Zr and ^{138}Ba . For the LUV
507 case, ^{55}Mn ranked higher than ^{46}Ti as the second most important element. The model also identified
508 elements that are exclusively important to each soil: ^{51}V in L22, ^{85}Rb in LUV and ^{89}Y in the ARZ
509 soil. Even though these are minor components in the fingerprint, the model does identify important
510 elements specific to each NNM.



511

512 Figure 5: Effect of soil type on the ability to classify ENMs and NNMs. ML results of the training

513 data for each test case (LUV + Ti100, ARZ + Ti100). Left scatter plots are only Ti-NNMs (L22)

514 displayed as the probability of the ML model predicting the correct category as a function of Ti

515 mass. Right scatter plots are the same but for only Ti-ENMs. Green represent Ti-NMs correctly

516 classified (> 85%) and orange is uncertain or misclassified (< 85%). The pie charts display the

517 percentage of total Ti-NMs categorized as correct (green), uncertain (orange), and incorrectly

518 classified (red).

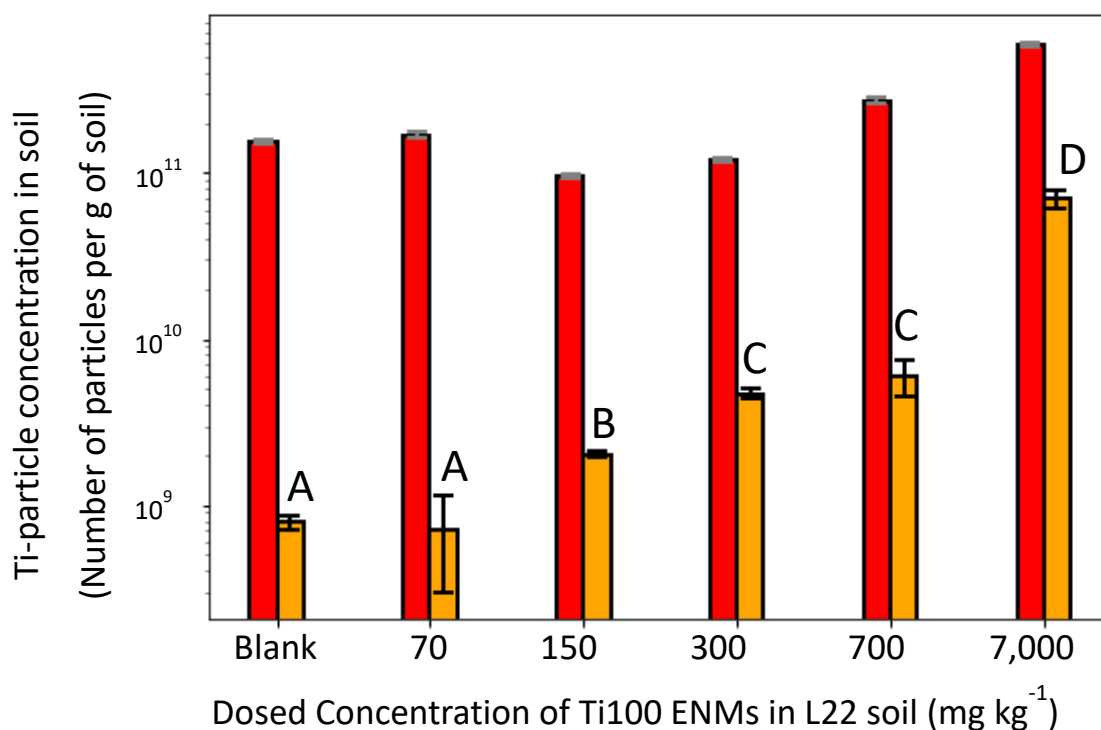
519 *Classifying Ti100 ENMs in dosed L22 soil*

520 We tested the ability of the trained ML model (Ti100 + L22) to classify the <500 nm sized

521 particles extracted from L22 soil dosed with Ti100 particles as either ENMs or NNMs. Five

522 different Ti100 ENM concentrations were used (70, 150, 300, 700, and 7,000 mg kg⁻¹) along with
523 an undosed (blank) soil to determine if the classification accuracy depended on particle
524 concentration. Recovered Ti-containing particle concentrations ranged from 9.7 x 10¹⁰ to 6.1 x
525 10¹¹ particles per g of soil (150 mg kg⁻¹ and 7,000 mg kg⁻¹ TiO₂, respectively). The number of
526 particles predicted as ENMs (> 85% probability) increased with increasing Ti100 concentration
527 (Figure 6). The amount of Ti100 added to the soil correlated to the total amount of Ti that was
528 extracted (Figure S22), suggesting that the extraction procedure was recovering the added Ti100
529 particles. From the blank, the total background Ti is approximately 1,600 mg kg⁻¹. Therefore, total
530 Ti recovery for dosed TiO₂ ENMs was not achieved for dosed concentrations lower than 7,000 mg
531 kg⁻¹. However, more Ti-containing particles were being recovered in dosed soils. At the highest
532 nominal concentration (7,000 mg kg⁻¹), the percent recovery of Ti was 36 ± 15 % by mass. This
533 highlights the value of spICP-TOFMS for identifying recovered individual Ti-containing particles
534 rather than total Ti in a sample. For the blank L22 soil, the model predicted low amounts of
535 particles labeled as ENMs (0.4%). These particles predicted as ENMs were unassociated with any
536 elements and had a mass distribution that is similar to the Ti100. There is not a statistically
537 significant increase in the predicted ENMs between the blank L22 and the soil with 70 mg kg⁻¹
538 TiO₂, but there is a difference between 70 mg kg⁻¹ and 150 mg kg⁻¹ amended soils, and between
539 150 mg kg⁻¹ and 300 mg kg⁻¹ (*P* value < 10⁻²). So, the detection limit for the Ti-100 ENMs in L22
540 is about 150 mg kg⁻¹. Current ENM emission models estimate 0.1 to 10 mg kg⁻¹ of nano TiO₂.
541 However, sludge and sludge-treated soil may exhibit higher concentrations that could be similar
542 to or exceeding the detection limit.^{40,53} A factor to consider in this estimate of the detection limit
543 is aging time. Using an aging time greater than 24 hours could lower the extraction efficiency of
544 the NMs from soil, thus increasing the ENM particle detection limit. A previous study performed

545 a similar experiment with CeO₂ ENMs dosed in soils and a trained ML model that included 17
546 other elements. Their ML model detected more ENMs in dosed soil with concentrations of 40 mg
547 kg⁻¹ and above.²⁸ This is not surprising given the distinction of Ce-based ENMs in soils is easier
548 because of the unique elemental fingerprint in Ce-NNMs (e.g., Ce + La) and the lower abundance
549 of Ce-NNMs in soil.



550
551 Figure 6: The ability to detect Ti100 ENMs dosed into L22 soil as a function of ENM
552 concentration. Ti particle concentration for each dosed Lufa soil: Blank (0 mg kg⁻¹), 70 mg kg⁻¹,
553 150 mg kg⁻¹, 300 mg kg⁻¹, 700 mg kg⁻¹, 7,000 mg kg⁻¹. Total Ti particle concentration is the red
554 bar. Orange bar represents the percentage of Ti-particles categorized as ENMs by the ML model
555 with a $\geq 85\%$ probability. Letters represent statistical similarity for one-way ANOVA (P value <
556 10⁻²). Sample size n = 3.

557 **Environmental Implications**

558 Currently, mass flow analysis models and fate and transport ENM models are used to
559 estimate ENM concentrations in the environment.^{15,25,53–55} While these models can be robust, they
560 cannot be easily validated because current analytical strategies cannot measure ENM
561 concentrations in relevant environment sinks (soil and sediments) at low concentration, especially
562 for ENMs made from earth-abundant elements that are some of the most common used ENMs.⁵⁶
563 The analytical strategy presented in this study is one of the first to detect and estimate
564 concentrations of a common ENM type (TiO₂) in soils and determine what NM properties makes
565 the ENMs distinguishable. This is a significant advancement towards validating existing fate and
566 transport ENM models. This analytical strategy can also potentially use elemental and mass
567 fingerprints to distinguish between specific ENM sources in the environment and determine ENM
568 source apportionment at impacted sites.

569 We assessed the efficacy of distinguishing Ti-based ENMs originating from three different
570 sources from NNMs in three different soil types using spICP-TOFMS and machine learning. The
571 majority of Ti-NNMs in soil are without elemental associations and distinguishing them from
572 ENMs is not possible using elemental fingerprints alone. However, machine learning models that
573 use both elemental information and mass distribution could positively identify ENMs in soils
574 except for Ti30 because of the limited elemental associations and the overlap in size with Ti-
575 containing NNMs. While not investigated here, the abundance of other relatively pure ENMs made
576 from earth abundant elements, e.g., iron oxides, may be similarly difficult to identify with
577 confidence depending on the mass distribution and elemental fingerprint of naturally occurring
578 iron oxides. For the Ti-sludge case, the model was able to distinguish a significant portion of the
579 Ti-sludge derived ENMs added to soil. It suggests that this approach could be applied to determine

580 the presence of Ti-sludge ENMs applied to agricultural soils. Detecting sludge NMs in agricultural
581 soil would imply their persistence in the environment and could lead to potential leachability in
582 surrounding water systems.⁵⁷

583 The ML models developed for this study identify specific elements and mass differences to
584 classify ENMs and NNMs. The models can learn ratios of similar associated elements to
585 differentiate ENMs and NNMs at a much deeper level than through observation alone. The ML
586 model simultaneously uses both elemental and size information, providing better classification
587 performance than using only elemental fingerprinting.

588 An important limitation of the supervised ML model is that it cannot yet be generalized to
589 identify a selected TiO₂ ENM in any soil. This is because it requires prior information on the
590 elemental and mass fingerprint on the ENMs of interest, and on the Ti-containing NNMs in the
591 soil prior to the introduction of ENMs. However, as with many ML approaches, creating a large,
592 shared dataset of fingerprints and mass distributions of Ti-containing NNMs from many different
593 soil types would create opportunities for classification and identification of ENMs in unknown
594 soils. Others have already implemented unsupervised learning methods to identify the elemental
595 fingerprints of NNMs in soil.³¹ With enough data on the range and types of background particle
596 types in many different soils, and the signature of the specific ENM of interest, a model may be
597 developed for broader applicability to a range of soils using these approaches. While the ML
598 models can classify some ENMs in soil, the lack of an elemental fingerprint in many of the NNMs,
599 and overlapping size distributions, makes it challenging to improve model accuracy for ENMs
600 made from earth abundant elements like Ti. A more distinct fingerprint of ENMs is needed. This
601 can be achieved by improving the detection limits of the spICP-TOFMS to increase the number of
602 associated elements that can be detected, or by enriching the ENM with a stable isotope to help

603 distinguish the ENM from background.⁵⁸⁻⁶⁰ These approaches could improve the ability to track
604 ENMs made from earth abundant elements in environmental systems by spICP-TOFMS of
605 extracted particles.

606 **Supporting Information**

607 ML Flowchart; NP Characterization; Soil Characterization and Experimental Design;
608 Hyper Parameter Tuning; Bootstrapping Method to Evaluate Sample Size; Isotopes that were
609 tracked with spICP-TOFMS; spICP-TOFMS parameters; Multi-elemental particle coincidence
610 and polyatomic interference; Mass distribution of Ti-NMs; Remaining ML Cases; Elemental
611 Fingerprint for each Test Case; Elemental Importance for each Test Case; The effect of H₂/He
612 mode as a collision cell gas on Ti classification; Investigating the effect of Al on Ti
613 classification; The effect of pretreating Ti30 sample on classification; Ti concentration measured
614 by ICP-OES

615 **Author Information**

616 Garret Bland: Carnegie Mellon University, Pittsburgh, PA, 15213, USA

617 Gregory Lowry* (Corresponding Author): Carnegie Mellon University, Pittsburgh, PA, 15213,
618 USA

619 Email: glowry@andrew.cmu.edu

620 Matthew Battifarano: Carnegie Mellon University, Pittsburgh, PA, 15213, USA

621 Ana Elena Pradas del Real: Madrid Institute for Agricultural Research (IMIDRA), N-II km 38,200,
622 28800 Alcala de Henares

623 Géraldine Sarret: ISTERre (Institut des Sciences de la Terre), Univ. Grenoble Alpes, CNRS, 38000,
624 Grenoble, France

625 **Acknowledgements**

626 This research is funded by the U.S. Army Research Office under grant # W911NF190063 to Greg
627 Lowry at CMU. The authors acknowledge use of the Materials Characterization Facility at
628 Carnegie Mellon University supported by grant MCF-677785. The authors would like to thank
629 Jonas Wielinski from Eawag – Swiss Federal Institute of Aquatic Science and Technology for
630 ICP-OES analysis. The authors would like to thank Dr. Josef Werne and Dr. Thomas Elliot Arnold
631 from University of Pittsburgh for the TOC analysis.

632 **References**

- 633 (1) Grieger, K. D.; Redmon, J. H.; Money, E. S.; Widder, M. W.; van der Schalie, W. H.;
634 Beaulieu, S. M.; Womack, D. A Relative Ranking Approach for Nano-Enabled
635 Applications to Improve Risk-Based Decision Making: A Case Study of Army Materiel.
636 *Environ. Syst. Decis.* **2015**, *35* (1), 42–53. <https://doi.org/10.1007/s10669-014-9531-4>.
- 637 (2) Sun, T. Y.; Mitrano, D. M.; Bornhöft, N. A.; Scheringer, M.; Hungerbühler, K.; Nowack,
638 B. Envisioning Nano Release Dynamics in a Changing World: Using Dynamic
639 Probabilistic Modeling to Assess Future Environmental Emissions of Engineered
640 Nanomaterials. *Environ. Sci. Technol.* **2017**, *51* (5), 2854–2863.
641 <https://doi.org/10.1021/acs.est.6b05702>.
- 642 (3) Praetorius, A.; Scheringer, M.; Hungerbühler, K. Development of Environmental Fate
643 Models for Engineered Nanoparticles - A Case Study of TiO₂ Nanoparticles in the Rhine
644 River. *Environ. Sci. Technol.* **2012**, *46* (12), 6705–6713.

645 <https://doi.org/10.1021/es204530n>.

646 (4) Loosli, F.; Wang, J.; Rothenberg, S.; Bizimis, M.; Winkler, C.; Borovinskaya, O.;
647 Flamigni, L.; Baalousha, M. Sewage Spills Are a Major Source of Titanium Dioxide
648 Engineered (Nano)-Particle Release into the Environment. *Environ. Sci. Nano* **2019**, *6* (3),
649 763–777. <https://doi.org/10.1039/c8en01376d>.

650 (5) Holden, P. A.; Gardea-Torresdey, J. L.; Klaessig, F.; Turco, R. F.; Mortimer, M.; Hund-
651 Rinke, K.; Cohen Hubal, E. A.; Avery, D.; Barceló, D.; Behra, R.; Cohen, Y.; Deydier-
652 Stephan, L.; Ferguson, P. L.; Fernandes, T. F.; Herr Harthorn, B.; Henderson, W. M.;
653 Hoke, R. A.; Hristozov, D.; Johnston, J. M.; Kane, A. B.; Kapustka, L.; Keller, A. A.;
654 Lenihan, H. S.; Lovell, W.; Murphy, C. J.; Nisbet, R. M.; Petersen, E. J.; Salinas, E. R.;
655 Scheringer, M.; Sharma, M.; Speed, D. E.; Sultan, Y.; Westerhoff, P.; White, J. C.;
656 Wiesner, M. R.; Wong, E. M.; Xing, B.; Steele Horan, M.; Godwin, H. A.; Nel, A. E.
657 Considerations of Environmentally Relevant Test Conditions for Improved Evaluation of
658 Ecological Hazards of Engineered Nanomaterials. *Environmental Science and*
659 *Technology*. American Chemical Society June 21, 2016, pp 6124–6145.
660 <https://doi.org/10.1021/acs.est.6b00608>.

661 (6) Giese, B.; Klaessig, F.; Park, B.; Kaegi, R.; Steinfeldt, M.; Wigger, H.; Von Gleich, A.;
662 Gottschalk, F. Risks, Release and Concentrations of Engineered Nanomaterial in the
663 Environment. *Sci. Rep.* **2018**, *8* (1), 1–18. <https://doi.org/10.1038/s41598-018-19275-4>.

664 (7) Fleischer, M.; Parker, R. L. Composition of the Earth's Crust. In *Data of Geochemistry*;
665 United States Government Printing Office, 1967.

666 (8) Gondikas, A.; Von Der Kammer, F.; Kaegi, R.; Borovinskaya, O.; Neubauer, E.;

- 667 Navratilova, J.; Praetorius, A.; Cornelis, G.; Hofmann, T. Where Is the Nano? Analytical
668 Approaches for the Detection and Quantification of TiO₂ Engineered Nanoparticles in
669 Surface Waters. *Environ. Sci. Nano* **2018**, *5* (2), 313–326.
670 <https://doi.org/10.1039/c7en00952f>.
- 671 (9) Navratilova, J.; Praetorius, A.; Gondikas, A.; Fabienke, W.; von der Kammer, F.;
672 Hofmann, T. Detection of Engineered Copper Nanoparticles in Soil Using Single Particle
673 ICP-MS. *Int. J. Environ. Res. Public Health* **2015**, *12* (12), 15756–15768.
674 <https://doi.org/10.3390/ijerph121215020>.
- 675 (10) Regelink, I. C.; Weng, L.; van Riemsdijk, W. H. The Contribution of Organic and Mineral
676 Colloidal Nanoparticles to Element Transport in a Podzol Soil. *Appl. Geochemistry* **2011**,
677 *26* (SUPPL.), S241–S244. <https://doi.org/10.1016/j.apgeochem.2011.03.114>.
- 678 (11) Tiede, K.; Boxall, A. B. A.; Tiede, D.; Tear, S. P.; David, H.; Lewis, J. A Robust Size-
679 Characterisation Methodology for Studying Nanoparticle Behaviour in “real”
680 Environmental Samples, Using Hydrodynamic Chromatography Coupled to ICP-MS. *J.*
681 *Anal. At. Spectrom.* **2009**, *24* (7), 964–972. <https://doi.org/10.1039/b822409a>.
- 682 (12) Spielman-Sun, E.; Lombi, E.; Donner, E.; Howard, D.; Unrine, J. M.; Lowry, G. V.
683 Impact of Surface Charge on Cerium Oxide Nanoparticle Uptake and Translocation by
684 Wheat (*Triticum Aestivum*). *Environ. Sci. Technol.* **2017**, *51* (13), 7361–7368.
685 <https://doi.org/10.1021/acs.est.7b00813>.
- 686 (13) Laughton, S.; Laycock, A.; von der Kammer, F.; Hofmann, T.; Casman, E. A.; Rodrigues,
687 S. M.; Lowry, G. V. Persistence of Copper-Based Nanoparticle-Containing Foliar Sprays
688 in *Lactuca Sativa* (Lettuce) Characterized by SpICP-MS. *J. Nanoparticle Res.* **2019**, *21*

- 689 (8). <https://doi.org/10.1007/s11051-019-4620-4>.
- 690 (14) Stampoulis, D.; Sinha, S. K.; White, J. C. Assay-Dependent Phytotoxicity of
691 Nanoparticles to Plants. *Environ. Sci. Technol.* **2009**, *43* (24), 9473–9479.
692 <https://doi.org/10.1021/es901695c>.
- 693 (15) Gottschalk, F.; Sun, T.; Nowack, B. Environmental Concentrations of Engineered
694 Nanomaterials: Review of Modeling and Analytical Studies. *Environmental Pollution*.
695 Elsevier Ltd October 1, 2013, pp 287–300. <https://doi.org/10.1016/j.envpol.2013.06.003>.
- 696 (16) Gallego-Urrea, J. A.; Tuoriniemi, J.; Pallander, T.; Hassellöv, M. Measurements of
697 Nanoparticle Number Concentrations and Size Distributions in Contrasting Aquatic
698 Environments Using Nanoparticle Tracking Analysis. *Environ. Chem.* **2010**, *7* (1), 67–81.
699 <https://doi.org/10.1071/EN09114>.
- 700 (17) Gimbert, L. J.; Haygarth, P. M.; Beckett, R.; Worsfold, P. J. Comparison of Centrifugation
701 and Filtration Techniques for the Size Fractionation of Colloidal Material in Soil
702 Suspensions Using Sedimentation Field-Flow Fractionation. *Environ. Sci. Technol.* **2005**,
703 *39* (6), 1731–1735. <https://doi.org/10.1021/es049230u>.
- 704 (18) Reed, R. B.; Martin, D. P.; Bednar, A. J.; Montañó, M. D.; Westerhoff, P.; Ranville, J. F.
705 Multi-Day Diurnal Measurements of Ti-Containing Nanoparticle and Organic Sunscreen
706 Chemical Release during Recreational Use of a Natural Surface Water. *Environ. Sci. Nano*
707 **2017**, *4* (1), 69–77. <https://doi.org/10.1039/c6en00283h>.
- 708 (19) Plathe, K. L.; Von Der Kammer, F.; Hasselov, M.; Moore, J.; Murayama, M.; Hofmann,
709 T.; Hochella, M. F. Using FIFFF and ATEM to Determine Trace Metalnanoparticle
710 Associations in Riverbed Sediment. *Environ. Chem.* **2010**, *7* (1), 82–93.

- 711 <https://doi.org/10.1071/EN091111>.
- 712 (20) Bolea, E.; Laborda, F.; Castillo, J. R. Metal Associations to Microparticles, Nanocolloids
713 and Macromolecules in Compost Leachates: Size Characterization by Asymmetrical Flow
714 Field-Flow Fractionation Coupled to ICP-MS. *Anal. Chim. Acta* **2010**, *661* (2), 206–214.
715 <https://doi.org/10.1016/J.ACA.2009.12.021>.
- 716 (21) Loosli, F.; Yi, Z.; Wang, J.; Baalousha, M. Dispersion of Natural Nanomaterials in
717 Surface Waters for Better Characterization of Their Physicochemical Properties by AF4-
718 ICP-MS-TEM. *Sci. Total Environ.* **2019**, *682*, 663–672.
719 <https://doi.org/10.1016/j.scitotenv.2019.05.206>.
- 720 (22) Zhou, X. X.; Liu, J. F.; Geng, F. L. Determination of Metal Oxide Nanoparticles and Their
721 Ionic Counterparts in Environmental Waters by Size Exclusion Chromatography Coupled
722 to ICP-MS. *NanoImpact* **2016**, *1*, 13–20. <https://doi.org/10.1016/j.impact.2016.02.002>.
- 723 (23) Degueldre, C.; Favarger, P. Y. Colloid Analysis by Single Particle Inductively Coupled
724 Plasma-Mass Spectroscopy: A Feasibility Study. In *Colloids and Surfaces A:
725 Physicochemical and Engineering Aspects*; Elsevier, 2003; Vol. 217, pp 137–142.
726 [https://doi.org/10.1016/S0927-7757\(02\)00568-X](https://doi.org/10.1016/S0927-7757(02)00568-X).
- 727 (24) Degueldre, C.; Favarger, P. Y.; Bitea, C. Zirconia Colloid Analysis by Single Particle
728 Inductively Coupled Plasma-Mass Spectrometry. *Anal. Chim. Acta* **2004**, *518* (1–2), 137–
729 142. <https://doi.org/10.1016/j.aca.2004.04.015>.
- 730 (25) Keller, A. A.; Lazareva, A. Predicted Releases of Engineered Nanomaterials: From Global
731 to Regional to Local. *Environ. Sci. Technol. Lett.* **2013**, *1* (1), 65–70.
732 <https://doi.org/10.1021/ez400106t>.

- 733 (26) Cornu, S.; Lucas, Y.; Lebon, E.; Ambrosi, J. P.; Luizão, F.; Rouiller, J.; Bonnay, M.;
734 Neal, C. Evidence of Titanium Mobility in Soil Profiles, Manaus, Central Amazonia.
735 *Geoderma* **1999**, *91* (3–4), 281–295. [https://doi.org/10.1016/S0016-7061\(99\)00007-5](https://doi.org/10.1016/S0016-7061(99)00007-5).
- 736 (27) Hendriks, L.; Gundlach-graham, A.; Günther, D. Analysis of Inorganic Nanoparticles by
737 Single-Particle Inductively Coupled Plasma Time-of-Flight Mass Spectrometry. *Chimia*
738 (*Aarau*). **2018**, *72* (4), 221–226. <https://doi.org/10.2533/chimia.2018.221>.
- 739 (28) Praetorius, A.; Gundlach-Graham, A.; Goldberg, E.; Fabienke, W.; Navratilova, J.;
740 Gondikas, A.; Kaegi, R.; Günther, D.; Hofmann, T.; Von Der Kammer, F. Single-Particle
741 Multi-Element Fingerprinting (SpMEF) Using Inductively-Coupled Plasma Time-of-
742 Flight Mass Spectrometry (ICP-TOFMS) to Identify Engineered Nanoparticles against the
743 Elevated Natural Background in Soils. *Environ. Sci. Nano* **2017**, *4* (2), 307–314.
744 <https://doi.org/10.1039/c6en00455e>.
- 745 (29) Green, T. H.; Pearson, N. J. An Experimental Study of Nb and Ta Partitioning between
746 Ti-Rich Minerals and Silicate Liquids at High Pressure and Temperature. *Geochim.*
747 *Cosmochim. Acta* **1987**, *51* (1), 55–62. [https://doi.org/10.1016/0016-7037\(87\)90006-8](https://doi.org/10.1016/0016-7037(87)90006-8).
- 748 (30) Gieré, R.; Williams, C. T. REE-Bearing Minerals in a Ti-Rich Vein from the Adamello
749 Contact Aureole (Italy). *Contrib. to Mineral. Petrol.* **1992**, *112* (1), 83–100.
750 <https://doi.org/10.1007/BF00310957>.
- 751 (31) Baalousha, M.; Wang, J.; Erfani, M.; Goharian, E. Elemental Fingerprints in Natural
752 Nanomaterials Determined Using SP-ICP-TOF-MS and Clustering Analysis. *Sci. Total*
753 *Environ.* **2021**, *792*, 148426. <https://doi.org/10.1016/J.SCITOTENV.2021.148426>.
- 754 (32) Mitra, S.; Datta, S.; Perkins, T.; Michailidis, G. *Introduction to Machine Learning and*

- 755 *Bioinformatics*; Taylor & Francis, 2008.
- 756 (33) Yang, X.; Liu, X.; Zhang, A.; Lu, D.; Li, G.; Zhang, Q.; Liu, Q.; Jiang, G. Distinguishing
757 the Sources of Silica Nanoparticles by Dual Isotopic Fingerprinting and Machine
758 Learning. *Nat. Commun.* **2019**, *10* (1). <https://doi.org/10.1038/s41467-019-09629-5>.
- 759 (34) Del Real, A. E. P.; Castillo-Michel, H.; Kaegi, R.; Sinnet, B.; Magnin, V.; Findling, N.;
760 Villanova, J.; Carrière, M.; Santaella, C.; Fernández-Martínez, A.; Levard, C.; Sarret, G.
761 Fate of Ag-NPs in Sewage Sludge after Application on Agricultural Soils. *Environ. Sci.*
762 *Technol.* **2016**, *50* (4), 1759–1768. <https://doi.org/10.1021/acs.est.5b04550>.
- 763 (35) Pradas del Real, A. E.; Castillo-Michel, H.; Kaegi, R.; Larue, C.; de Nolf, W.; Reyes-
764 Herrera, J.; Tucoulou, R.; Findling, N.; Salas-Colera, E.; Sarret, G. Searching for Relevant
765 Criteria to Distinguish Natural vs. Anthropogenic TiO₂ Nanoparticles in Soils. *Environ.*
766 *Sci. Nano* **2018**, *5* (12), 2853–2863. <https://doi.org/10.1039/C8EN00386F>.
- 767 (36) Lahive, E.; Matzke, M.; Durenkamp, M.; Lawlor, A. J.; Thacker, S. A.; Pereira, M. G.;
768 Spurgeon, D. J.; Unrine, J. M.; Svendsen, C.; Lofts, S. Sewage Sludge Treated with Metal
769 Nanomaterials Inhibits Earthworm Reproduction More Strongly than Sludge Treated with
770 Metal Metals in Bulk/Salt Forms. *Environ. Sci. Nano* **2017**, *4* (1), 78–88.
771 <https://doi.org/10.1039/C6EN00280C>.
- 772 (37) Bland, G. D.; Lowry, G. V. Multi-Step Method to Extract Moderately Soluble Copper
773 Oxide Nanoparticles from Soil for Quantification and Characterization. *Anal. Chem.* **2020**,
774 *92* (14), 9620–9628. <https://doi.org/10.1021/acs.analchem.0c00824>.
- 775 (38) Pandorf, M.; Pourzahedi, L.; Gilbertson, L.; Lowry, G. V.; Herckes, P.; Westerhoff, P.
776 Graphite Nanoparticle Addition to Fertilizers Reduces Nitrate Leaching in Growth of

- 777 Lettuce (*Lactuca Sativa*). *Environ. Sci. Nano* **2020**, 7 (1), 127–138.
778 <https://doi.org/10.1039/C9EN00890J>.
- 779 (39) Gao, X.; Spielman-Sun, E.; Rodrigues, S. M.; Casman, E. A.; Lowry, G. V. Time and
780 Nanoparticle Concentration Affect the Extractability of Cu from CuO NP-Amended Soil.
781 *Environ. Sci. Technol.* **2017**, 51 (4), 2226–2234. <https://doi.org/10.1021/acs.est.6b04705>.
- 782 (40) Sun, T. Y.; Bornhöft, N. A.; Hungerbühler, K.; Nowack, B. Dynamic Probabilistic
783 Modeling of Environmental Emissions of Engineered Nanomaterials. *Environ. Sci.*
784 *Technol.* **2016**, 50 (9), 4701–4711. <https://doi.org/10.1021/ACS.EST.5B05828>.
- 785 (41) Pace, H. E.; Rogers, N. J.; Jarolimek, C.; Coleman, V. A.; Higgins, C. P.; Ranville, J. F.
786 Determining Transport Efficiency for the Purpose of Counting and Sizing Nanoparticles
787 via Single Particle Inductively Coupled Plasma Mass Spectrometry. *Anal. Chem.* **2011**, 83
788 (24), 9361–9369. <https://doi.org/10.1021/ac201952t>.
- 789 (42) Tanner, M.; Günther, D. Short Transient Signals, a Challenge for Inductively Coupled
790 Plasma Mass Spectrometry, a Review. *Analytica Chimica Acta*. Elsevier February 2, 2009,
791 pp 19–28. <https://doi.org/10.1016/j.aca.2008.11.041>.
- 792 (43) Venkatesan, A. K.; Reed, R. B.; Lee, S.; Bi, X.; Hanigan, D.; Yang, Y.; Ranville, J. F.;
793 Herckes, P.; Westerhoff, P. Detection and Sizing of Ti-Containing Particles in
794 Recreational Waters Using Single Particle ICP-MS. *Bull. Environ. Contam. Toxicol.* **2018**,
795 100 (1), 120–126. <https://doi.org/10.1007/s00128-017-2216-1>.
- 796 (44) Dan, Y.; Shi, H.; Stephan, C.; Liang, X. Rapid Analysis of Titanium Dioxide
797 Nanoparticles in Sunscreens Using Single Particle Inductively Coupled Plasma–Mass
798 Spectrometry. *Microchem. J.* **2015**, 122, 119–126.

- 799 <https://doi.org/10.1016/J.MICROC.2015.04.018>.
- 800 (45) Liu, D. C.; Nocedal, J. On the Limited Memory BFGS Method for Large Scale
801 Optimization. *Math. Program.* **1989**, *45* (1–3), 503–528.
802 <https://doi.org/10.1007/BF01589116>.
- 803 (46) Wielinski, J.; Gogos, A.; Voegelin, A.; Müller, C.; Morgenroth, E.; Kaegi, R.
804 Transformation of Nanoscale and Ionic Cu and Zn during the Incineration of Digested
805 Sewage Sludge (Biosolids). *Environ. Sci. Technol.* **2019**, *53* (20), 11704–11713.
806 <https://doi.org/10.1021/acs.est.9b01983>.
- 807 (47) Weaver, C. E. The Nature of TiO₂ in Kaolinite. *Clays Clay Miner.* **1976**, *24* (5), 215–218.
808 <https://doi.org/10.1346/ccmn.1976.0240501>.
- 809 (48) Cornu, S.; Lucas, Y.; Lebon, E.; Ambrosi, J. P.; Luizão, F.; Rouiller, J.; Bonnay, M.;
810 Neal, C. Evidence of Titanium Mobility in Soil Profiles, Manaus, Central Amazonia.
811 *Geoderma* **1999**, *91* (3–4), 281–295. [https://doi.org/10.1016/S0016-7061\(99\)00007-5](https://doi.org/10.1016/S0016-7061(99)00007-5).
- 812 (49) Van Baalen, M. R. Titanium Mobility in Metamorphic Systems: A Review. *Chem. Geol.*
813 **1993**, *110* (1–3), 233–249. [https://doi.org/10.1016/0009-2541\(93\)90256-I](https://doi.org/10.1016/0009-2541(93)90256-I).
- 814 (50) Philippe, A.; Campos, D. A.; Guigner, J.-M.; Buchmann, C.; Diehl, D.; Schaumann, G. E.
815 Characterization of the Natural Colloidal TiO₂ Background in Soil. *Sep. 2018, Vol. 5*,
816 *Page 50* **2018**, *5* (4), 50. <https://doi.org/10.3390/SEPARATIONS5040050>.
- 817 (51) Azimzada, A.; Farner, J. M.; Jreije, I.; Hadioui, M.; Liu-Kang, C.; Tufenkji, N.; Shaw, P.;
818 Wilkinson, K. J. Single- and Multi-Element Quantification and Characterization of TiO₂
819 Nanoparticles Released From Outdoor Stains and Paints. *Front. Environ. Sci.* **2020**, *8*, 91.

- 820 <https://doi.org/10.3389/fenvs.2020.00091>.
- 821 (52) Praetorius, A.; Badetti, E.; Brunelli, A.; Clavier, A.; Gallego-Urrea, J. A.; Gondikas, A.;
822 Hassellöv, M.; Hofmann, T.; Mackevica, A.; Marcomini, A.; Peijnenburg, W.; Quik, J. T.
823 K.; Seijo, M.; Stoll, S.; Tepe, N.; Walch, H.; Von Der Kammer, F. Strategies for
824 Determining Heteroaggregation Attachment Efficiencies of Engineered Nanoparticles in
825 Aquatic Environments. *Environ. Sci. Nano* **2020**, *7* (2), 351–367.
826 <https://doi.org/10.1039/c9en01016e>.
- 827 (53) Sun, T. Y.; Gottschalk, F.; Hungerbühler, K.; Nowack, B. Comprehensive Probabilistic
828 Modelling of Environmental Emissions of Engineered Nanomaterials. *Environ. Pollut.*
829 **2014**, *185*, 69–76. <https://doi.org/10.1016/j.envpol.2013.10.004>.
- 830 (54) Gottschalk, F.; Nowack, B. The Release of Engineered Nanomaterials to the Environment.
831 *Journal of Environmental Monitoring*. May 2011, pp 1145–1155.
832 <https://doi.org/10.1039/c0em00547a>.
- 833 (55) Garner, K. L.; Suh, S.; Keller, A. A. Assessing the Risk of Engineered Nanomaterials in
834 the Environment: Development and Application of the NanoFate Model. *Environ. Sci.*
835 *Technol.* **2017**, *51* (10), 5541–5551. <https://doi.org/10.1021/acs.est.6b05279>.
- 836 (56) Dale, A. L.; Casman, E. A.; Lowry, G. V.; Lead, J. R.; Viparelli, E.; Baalousha, M.
837 Modeling Nanomaterial Environmental Fate in Aquatic Systems. *Environ. Sci. Technol.*
838 **2015**, *49* (5), 2587–2593. <https://doi.org/10.1021/es505076w>.
- 839 (57) Brar, S. K.; Verma, M.; Tyagi, R. D.; Surampalli, R. Y. Engineered Nanoparticles in
840 Wastewater and Wastewater Sludge - Evidence and Impacts. *Waste Management*.
841 Pergamon March 1, 2010, pp 504–520. <https://doi.org/10.1016/j.wasman.2009.10.012>.

- 842 (58) Laycock, A.; Diez-Ortiz, M.; Larner, F.; Dybowska, A.; Spurgeon, D.; Valsami-Jones, E.;
843 Rehkämper, M.; Svendsen, C. Earthworm Uptake Routes and Rates of Ionic Zn and ZnO
844 Nanoparticles at Realistic Concentrations, Traced Using Stable Isotope Labeling. *Environ.*
845 *Sci. Technol.* **2016**, *50* (1), 412–419. <https://doi.org/10.1021/acs.est.5b03413>.
- 846 (59) Larner, F.; Dogra, Y.; Dybowska, A.; Fabrega, J.; Stolpe, B.; Bridgestock, L. J.;
847 Goodhead, R.; Weiss, D. J.; Moger, J.; Lead, J. R.; Valsami-Jones, E.; Tyler, C. R.;
848 Galloway, T. S.; Rehkämper, M. Tracing Bioavailability of ZnO Nanoparticles Using
849 Stable Isotope Labeling. *Environ. Sci. Technol.* **2012**, *46* (21), 12137–12145.
850 <https://doi.org/10.1021/es302602j>.
- 851 (60) Larner, F.; Gulson, B.; McCall, M.; Oytam, Y.; Rehkämper, M. An Inter-Laboratory
852 Comparison of High Precision Stable Isotope Ratio Measurements for Nanoparticle
853 Tracing in Biological Samples. *J. Anal. At. Spectrom.* **2014**, *29* (3), 471–477.
854 <https://doi.org/10.1039/c3ja50322d>.

855